



# Synthesis of the novel binary composite of self-suspended polyaniline (S-PANI) and functionalized multi-walled carbon nanotubes for high-performance supercapacitors

Abdul Rehman Akbar<sup>1</sup> · Jinxing Wu<sup>1</sup> · Muhammad Tahir<sup>1</sup> · Huihui Hu<sup>1</sup> · Chen Yu<sup>1</sup> · Muhammad Bilal Qadir<sup>2</sup> · Fahad Mateen<sup>3</sup> · Chuanxi Xiong<sup>1</sup> · Quanling Yang<sup>1</sup>

Received: 29 October 2020 / Revised: 13 January 2021 / Accepted: 14 January 2021 / Published online: 1 February 2021  
© The Author(s), under exclusive licence to Springer-Verlag GmbH, DE part of Springer Nature 2021

## Abstract

To push the upper limit of capacitive materials, the integration of multi-modal capacitive materials has emerged as a potential solution. In this regard, we reported the novel binary composite of self-suspended polyaniline (S-PANI) and multi-walled carbon nanotubes (MWNTs). Compared with conventional polyaniline, S-PANI offers higher porosity and fibrillar polymeric network, which was achieved by doping long-chain protonic acid during in situ polymerization. S-PANI was loaded on oxidized carbon nanotubes (OCNTs) and sulfonated carbon nanotubes (SCNTs) to prepare S-PANI/OCNT and S-PANI/SCNT composite electrodes, respectively. The conductive and exclusive fibrillar S-PANI provide unobstructed channels for charge transport and electrolyte infiltration. Preliminary electrochemical studies revealed that the capacitance of the composite electrode reached  $316.8 \text{ F g}^{-1}$  and  $345.4 \text{ F g}^{-1}$ , and established exceptional capacitance retention rates of 92.8% and 93.7% after 5000 cycles for S-PANI/OCNT and S-PANI/SCNT composite, respectively, making it a potential candidate for imminent energy storage devices.

**Keywords** Optimized binary composite · Multi-walled carbon nanotubes · Solvent-free polyaniline (S-PANI) · Supercapacitor · Electrochemical characteristics

## Introduction

Energy storage is considered as a major issue faced by humanity, specifically for emerging renewable energy resources. Highly reliable energy storage devices with long cycle life, proficient performance, and low cost have been the center of research in recent years [1, 2]. To meet the high demand for energy storage, several different devices have been deployed

such as batteries and supercapacitors (SCs) [3–5]. SCs have emerged as an attractive owing to its distinctive features, such as long-lasting cycle life, higher power densities, and high charge-discharge speed. Therefore, SCs have been utilized in several fields like electronic vehicles, mobile devices, and automobiles [6–8]. SCs are further classified into electric double-layer capacitors (EDLCs), a pseudocapacitor (PC), or a hybrid SC. EDLCs dominantly include carbon materials that are characterized by their electrostatic ion adsorption/desorption at the electrode/electrolyte interface for charge and discharge, respectively. PCs using conducting polymers or transition metal oxides (NiO, Fe<sub>2</sub>O<sub>3</sub>, Fe<sub>3</sub>O<sub>4</sub>, etc.) are characterized by rapid redox reactions occurring on the surface of the electrodes [9–14]. Both EDLCs and PCs have certain limitations of limited performance and limited stability, respectively. In order to overcome these limitations, a suitable composite structure of carbon materials and polymers can effectively integrate high performance and stability in single composite structure [15–18].

Carbon-based materials specifically multi-walled carbon nanotubes (MWCNTs) have been widely employed in

✉ Chuanxi Xiong  
cxiong@whut.edu.cn

✉ Quanling Yang  
yangql@whut.edu.cn

<sup>1</sup> State Key Laboratory of Silicate Materials for Architectures, and School of Materials Science and Engineering, Wuhan University of Technology, Wuhan 430070, China

<sup>2</sup> Faculty of Engineering & Technology, National Textile University, Faisalabad 37610, Pakistan

<sup>3</sup> Department of Chemical and Biochemical Engineering, Dongguk University, 100-715 Seoul, South Korea

EDLCs due to their intrinsic properties of a larger specific area, low cost, lower toxicity, abundance, higher cycling stability, and environmentally friendly nature [19–23]. Among EDLCs, MWCNTs got substantial attraction owing to specific characteristics of the entangled network, special porous characteristics, and superior electrical conductivity [24]. However, to unlock complete potential of MWCNTs, a suitable dispersion is necessary, as bare MWCNTs are readily aggregated and lose their performance. For this purpose, the functionalization of heteroatoms has been investigated for their superior dispersion and higher EC performance [25–32]. The electric double-layer specific capacitance is dependent upon the electrostatic accumulation of charges in the electric double layer; therefore, improving the specific surface area, electrical conductance, and structural stability of the electrode materials significantly endorses positive effects on the electrochemical characteristics [33]. To enhance the MWCNT characteristics, they have been treated in various ways, such as functionalizing, coating, oxidizing, and filling the pristine nanotubes [34]. MWCNT needs to go through supplementary treatments to functionalize the composites irrespective of their exceptional properties. The pristine MWCNT could be purified further, and oxygen-containing groups would be introduced on the surface after treatment to assist the exfoliation of MWCNT packs and enhance the solubility in polar media. Functionalizing the nanotubes affects their processing and enables the modification/functionalization possibility to form the desired MWCNT composite [35, 36].

In general, conducting polymer-based PCs exhibit superior energy density than the EDLCs [37]. The conducting polymers have distinctive features such as high power capability, lower cost, and superior charge density. Various conducting polymers have been employed and studied in SCs such as polyaniline (PANI) and polypyrrole [26, 38–42]. The PANI offers a high theoretical specific capacitance, excellent redox reaction behavior, easy availability of raw materials, and low cost, hence most widely used. However, the PANI suffers from its efficient consumption and low solubility. The different oxidation states of PANI affect the conductance and EC performance of the polymer. This issue could be resolved by doping the optimum concentration of dopant or by controlling its structure during synthesis or combining it with materials having superior mechanical properties [43, 44]. In this regard, MWCNTs hold great potential as a dopant, thanks to their mechanical and electronic characteristics [45]. Despite adding MWCNTs in the polymeric network, the capacitance is still limited due to the limited porosity of PANI. To overcome this critical bottleneck, we proposed a unique porous architecture self-suspended PANI (S-PANI), which offers a higher surface area, hence resulting in superior capacitance. The S-PANI was synthesized by doping long-chain protonic acid, sodium nonylphenol polyoxyethylene ether sulfate (NPES), during in situ polymerization. In S-PANI, the doped derivatives self-assemble into nanofibrils. By controlling the doping ratio

of PANI molecular chains in the system, micelles can be further formed to obtain higher specific surface area (SSA) and ultimately improve performance. S-PANI is completely different from previously reported because it comprises distinctive fibrillar network morphology. The prepared S-PANI has excellent electrical conductivity, excellent water solubility, light weight and distinctive porous flow structures. The unique fiber structure improves the conductivity of the composite aerogel and reduces the ion diffusion resistance. The introduction of S-PANI noticeably enhanced the dispersion and gave full play to composite's pseudopotentiability [46].

In this study, the unique solvent-free S-PANI nanoscale fluid was prepared through long-chain protonic acid, sodium nonylphenol polyoxyethylene ether sulfate (NPES), during in situ polymerization. The MWCNTs were pretreated by the mixed acid oxidation method and the diazonium salt method to obtain oxidized carbon nanotubes (OCNTs) with (–OH, –COOH) active functional groups and sulfonated carbon nanotubes (SCNTs) with sulfonic acid groups. The S-PANI was compounded with functionalized OCNT and SCNT to make binary S-PANI/OCNT and S-PANI/SCNT composite supercapacitor electrodes. The organic long chains on the surface of S-PANI endowed it with good water solubility, enabling it to be fully dissolved in an aqueous solution with functionalized MWCNTs. Subsequently, we used the mixed aqueous solution of S-PANI and functionalized MWCNTs as the precursor, and obtained the corresponding composite material by one-step self-assembly by hydrothermal method. The chemical structure and micromorphology of S-PANI/OCNT and S-PANI/SCNT were characterized by a variety of testing methods, and their electrochemical properties were tested as active electrode materials. This strategy helped to develop an efficient SC with stable and longer cyclic life. The results specified that proposed binary composites are high-performance electrode materials for supercapacitors.

## Experimental section

### Materials

Nonylphenol ethoxylate sulfonate-10 (NPES-10) and 4-aminobenzenesulfonic acid ( $C_6H_7NO_3S$ ) were bought from Sigma-Aldrich Chemical Reagent Company. Aniline ( $C_6H_5NH_2$ ) and acetone ( $CH_3COCH_3$ ) all were acquired from Shanghai Aladdin Biochemical Technology Co., Ltd with 99.9% analytical purity. Ammonium persulfate ( $(NH_4)_2S_2O_8$ ), nitric acid ( $HNO_3$ , 65%), sulfuric acid ( $H_2SO_4$ , 98%), sodium hydroxide (NaOH), sodium nitrite ( $NaNO_2$ ), ethanol ( $C_2H_5OH$ ), *N,N*-dimethylformamide (DMF), potassium chloride (KCl), MWCNT, perfluorosulfonic acid polytetrafluoroethylene solution (Nafion 5% W/W), and alumina powder ( $Al_2O_3$ ) all in analytically pure form purchased

from Sinopharm Chemical Reagent Co., Ltd. All chemicals were attained and exposed to use deprived of additional purification.

### Preparation of solvent-free self-suspended polyaniline fluid

The S-PANI was prepared by following our previous work [46]. First, the 250-mL three-neck flask was immersed in ethanol in the cryostat and the temperature was adjusted to 0 °C. Then, 14.55 g of NPES (0.012 mol) was added into 80 mL deionized water and stirred until the NPES is completely dissolved. This NPES was transferred to the three-neck flask. Aniline, 1.86 g was dispersed in 5 mL of deionized water, then added it dropwise to the above solution under continuous stirring for 30 min. Secondly, a solution of 4.56 g ammonium persulfate dissolved in 20 mL deionized water was added to the three-neck flask solution and mixed solution for 1 h. During the reaction, the temperature was kept below 3 °C. After 8 h of reaction, the product was ultrasonically demulsified for 10 min, and then, vacuum filtration was performed to obtain the filtrate in the suction flask. To remove impurities, the brown liquid filtrate in the suction flask was assembled with a cellulose dialysis bag (MW-8000 Da) and placed in circulating water for dialysis for 72 h. The dialyzed liquid was transferred to a beaker and dried in an oven at 80 °C for 6 h to obtain purified S-PANI.

### Preparation of oxidized carbon nanotubes

The CNT (1 g) was dispersed in a pre-configured 200 mL mixed acid (the volume ratio of HNO<sub>3</sub>/H<sub>2</sub>SO<sub>4</sub> is 1:3) and diluted to 500 mL with deionized water after continuous ultrasonic oxidation for 3 h. The reaction solution was transferred to multiple centrifuge tubes, centrifuged at 8000 r/min for 20 min, and the precipitate was taken. The above operation was repeated, and deionized water was added cautiously to dilute the precipitate until the pH value of the last centrifuge is 3. The product was then transferred to a beaker and dried at 80 °C to obtain oxidized carbon nanotubes, which were labeled as OCNT.

### Preparation of sulfonated carbon nanotubes

A 250-mL three-necked flask was adjusted into a low-temperature thermostat preset at 3 °C, and 3.4 g of 4-aminobenzenesulfonic acid was added into it under continuous stirring followed by adding NaOH solution (5wt%, 20 mL) dropwise. The temperature of the solution was raised to 50 °C and stirred at a constant speed until the solution is transparent. The stirring was continued for 15 min, and NaNO<sub>2</sub> solution (1 mol/L, 20 mL) was added dropwise. When the system temperature dropped to 3 °C, the pre-

prepared dilute hydrochloric acid (1 mol/L) was added dropwise. The reaction liquid gradually changed from light yellow to light brown. The diluted hydrochloric acid was continually added until the reaction liquid turned creamy yellow. A total of 45 mL diluted hydrochloric acid is added dropwise, and the reaction is continued for 30 min to obtain the diazonium salt solution. Afterwards, 0.4 g of MWCNT has added it to the reaction solution, and stirring was sustained for 2 h, and then, the three-neck flask was removed. The solution was uninterruptedly stirred at room temperature 25 °C for 24 h. The solution was vacuum filtered and washed with deionized water several times until the filtrate is colorless and transparent. The filter cake was transported to a beaker and dried at 80 °C to obtain the final product of sulfonated carbon nanotubes, which was referred to as SCNT.

### Preparation of S-PANI/OCNT and S-PANI/SCNT composite materials

To prepare composite, 0.2 g of S-PANI and 0.1 g of OCNT were dispersed in 50 mL deionized water, and then dispersed the mixture ultrasonically for 10 min, and transferred it to a three-neck flask. The temperature of the constant temperature water tank was set to 5 °C, and the three-neck flask was moved to it and stirred for 24 h. Suction filtration was performed, and the filtrate was washed with deionized water 3–5 times to obtain the final product, which was dried at 80 °C to obtain S-PANI/OCNT composite 1. The S-PANI/SCNT composite material was obtained by repeating the above experimental steps except replacing SCNT with OCNT.

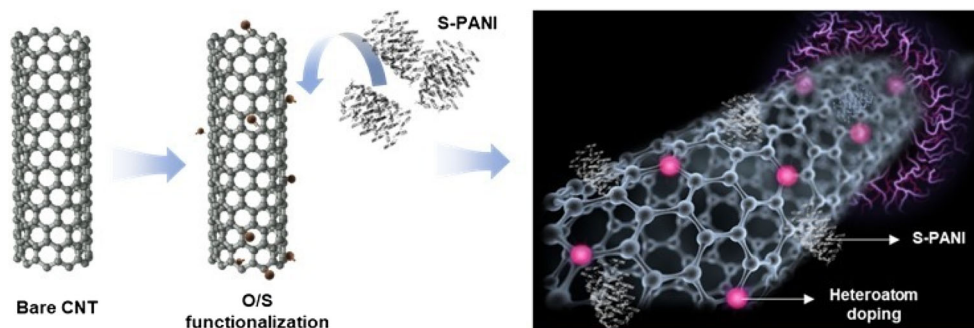
### Preparation of working electrode

The as-prepared S-PANI/OCNT and S-PANI/SCNT composite materials were prepared into the working electrode. Acetylene black and active material were dispersed in 1 mL DMF at a mass ratio of 1:8; then, 5 µL of Nafion solution with a mass ratio of 5 wt% was added to the dispersion, and magnetically stirred for 2 h to make uniform dispersion. Before the test, the surface of the glassy carbon electrode was polished with Al<sub>2</sub>O<sub>3</sub> powder with a diameter of 50 nm, and then, the surface of the glassy carbon electrode was rinsed with deionized water, acetone, and ethanol. The final electrode surface showed a mirror gloss. Afterwards, 1.5 µL of the pre-prepared dispersion solution was coated on the 1.5-mm-diameter electrode area by drop casting method. Coated electrode was subjected to vacuum drying oven to remove DMF followed by electrochemical testing (Scheme 1).

### Characterization

The Fourier transform infrared spectrometer (FT-IR) from Thermo Nicolet, USA, was used to characterize the chemical

**Scheme 1** Schematic illustration for preparation of S-PANI-based binary composite electrodes



structure of different samples. The samples were mixed with KBr powder, grounded, and pressed into tablets with a test spectrum range of 4000–500  $\text{cm}^{-1}$ . The X-ray diffractometer (German Bruker, D8 advance) was used to analyze the phase of each sample with scanning range  $2\theta = 5\text{--}70^\circ$ . The Raman spectroscopy of each sample was tested with a confocal Raman microscope (British, RENISHAW) equipped with 514.5-nm argon ion laser. The Zeiss Ultra Plus (Germany) field emission scanning electron microscope (SEM) was used to observe the surface micromorphology of different samples. The specific surface area and pore size distribution of the sample were tested using the porosity analyzer of the American Mike company model (ASAP 2020M). The  $\text{N}_2$  was used as adsorption gas. Three-electrode system was used for EC performance analysis. The electrochemical workstation model CHI 660E (Shanghai Chenhua) was used to test the cyclic voltammetry (CV) characteristics, galvanostatic charge/discharge (GCD), cycle stability performance, and electrochemical AC impedance of each electrode material. The Ag/AgCl reference electrode, the platinum wire counter electrode, and the S-PANI/OCNT and S-PANI/SCNT composite materials were used as the working electrode.

## Results and discussion

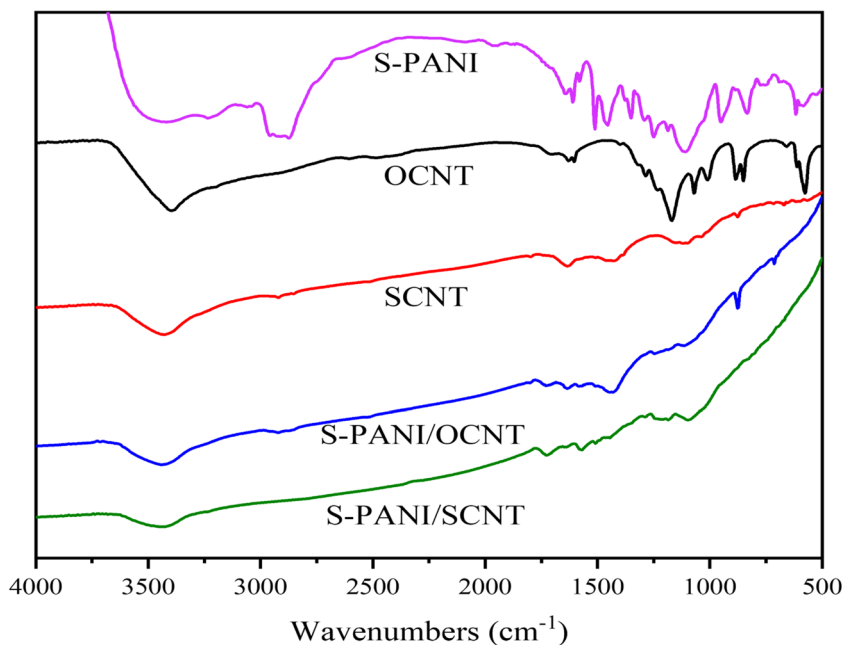
In order to analyze the molecular structure of the substance and to determine the functional groups, FT-IR spectroscopy was conducted as shown in Fig. 1. Because the branched NPES grafted on polyaniline contains multiple functional groups, the FT-IR spectrum of S-PANI has multiple characteristic peaks in the range of 500  $\text{cm}^{-1}$  to 2000  $\text{cm}^{-1}$ . For OCNT, strong characteristic peaks appear at 3396  $\text{cm}^{-1}$ , 1621  $\text{cm}^{-1}$ , 1169  $\text{cm}^{-1}$ , and 1070  $\text{cm}^{-1}$ , which proved the introduction of  $-\text{OH}$  and  $-\text{COOH}$  functional groups under the treatment of mixed acid. The characteristic peaks of SCNT at 1634  $\text{cm}^{-1}$  and 1478  $\text{cm}^{-1}$  correspond to  $\text{C}=\text{O}$  bond stretching vibration and  $\text{N}-\text{H}$  bond bending vibration. Besides, the characteristic peaks at 1044  $\text{cm}^{-1}$  and 1121  $\text{cm}^{-1}$  belong to the  $\text{S}-\text{O}$  bond on the  $-\text{SO}_3$  group. It can be seen from the figure that the characteristic peak intensity of S-

PANI/OCNT and S-PANI/SCNT in the 1800–1000  $\text{cm}^{-1}$  band became weaker. This is because the active functional groups on the surface of S-PANI and OCNT and SCNT are strong. Interaction and new covalent bonds were generated. Among them, the characteristic peak at 2920  $\text{cm}^{-1}$  is attributed to the  $\text{C}-\text{H}$  bonds in  $-\text{CH}_2-$  and  $-\text{CH}_3$  on the grafted flexible branch, while the characteristic peak at about 3470  $\text{cm}^{-1}$  proved the existence of alcoholic hydroxyl groups on the carbon chain. These characteristics peaks also indicated that S-PANI was incorporated into activated carbon nanotubes.

The X-ray diffraction (XRD) was conducted to analyze the internal structure changes of the composite, as shown in Fig. 2. It can be seen that both OCNT and SCNT have two broad peaks at about  $26^\circ$  and  $44^\circ$ , which correspond to (002) and (100) crystal planes of carbon materials, which are the same as those of pure carbon nanotubes. The XRD curve of S-PANI only shows a broad peak at  $20.9^\circ$ , indicating a dominantly amorphous structure. In general, the crystal faces of S-PANI/OCNT and S-PANI/SCNT are the same as those of CNTs, in which (002) crystal plane slightly deviates at a lower angle compared with OCNT or SCNT, and (100) crystal plane strength decreases. However, the diffraction peak corresponding to S-PANI in the composite material disappeared, which also explained to a certain extent that there might be an interaction force between S-PANI and MWCNT.

To further characterize the structural defects of S-PANI/OCNT and S-PANI/SCNT, the Raman spectroscopy tests were performed on each sample and compared it with OCNT and SCNT, as shown in Fig. 3. In the Raman characteristic peaks of carbon materials, D band and G band were located at wavenumbers of 1300  $\text{cm}^{-1}$  and 1580  $\text{cm}^{-1}$ , respectively. The D band represents the disorder and lattice defects, and the G band represents ideally crystalline ( $\text{sp}^2$  carbon) structure. In comparison with OCNT and SCNT, the D bands of S-PANI/OCNT and S-PANI/SCNT have moved from 1332  $\text{cm}^{-1}$  and 1330  $\text{cm}^{-1}$  to 1323  $\text{cm}^{-1}$ , respectively. The G band shifted from 1583  $\text{cm}^{-1}$  and 1580  $\text{cm}^{-1}$  to 1573  $\text{cm}^{-1}$ , respectively. This is due to the introduction of a large number of organic functional groups after the composite of carbon nanotubes and S-PANI.

**Fig. 1** FTIR spectra of S-PANI, OCNT, SCNT, S-PANI/OCNT, and S-PANI/SCNT



$I_D/I_G$  is the intensity ratio of peak D and peak G, reflecting the intensity relationship between these two peaks. The higher the ratio, the more lattice defects of carbon atoms. The  $I_D/I_G$  intensity ratio values of OCNT, SCNT, S-PANI/OCNT, and S-PANI/SCNT are 1.13, 1.06, 1.37, and 1.27, respectively. The  $I_D/I_G$  of composite structure materials S-PANI/OCNT and S-PANI/SCNT are both higher than that of OCNT and SCNT. It is of the pore volume and three-dimensionality

degree of the samples that has increased to a certain level after being composited with S-PANI. Besides, defect-rich morphology of S-PANI, which is an integral component of the composite also contributed to it.

The porous morphology has a strong influence on the electrochemical performance of materials. Higher SSA and porosity facilitate the transport of ions through the symmetry of the electrode, thus resulting in an excellent electrochemical

**Fig. 2** XRD patterns of OCNT, SCNT, S-PANI/OCNT, S-PANI/SCNT, and S-PANI

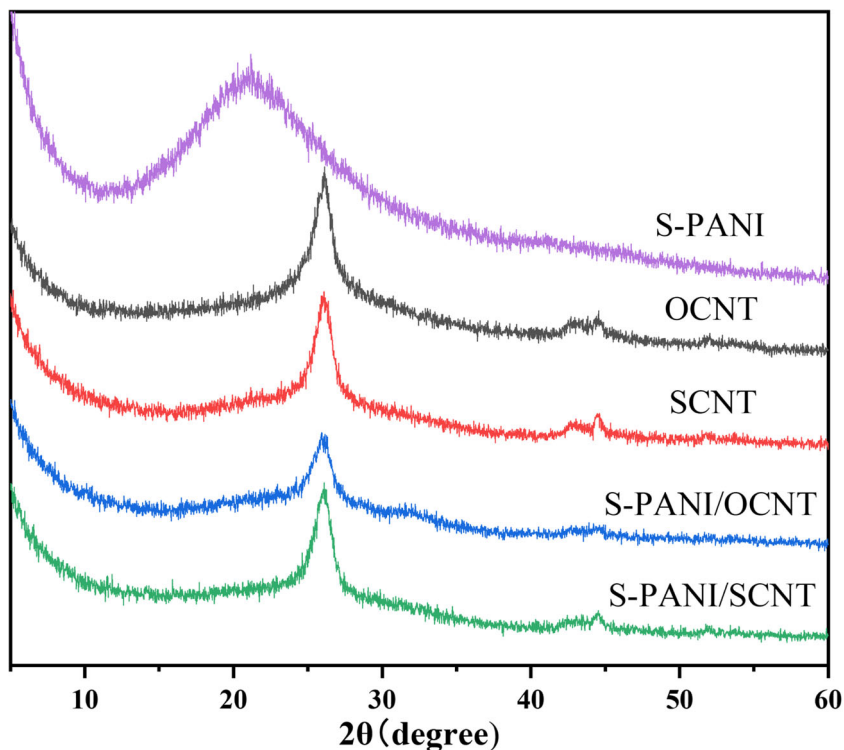
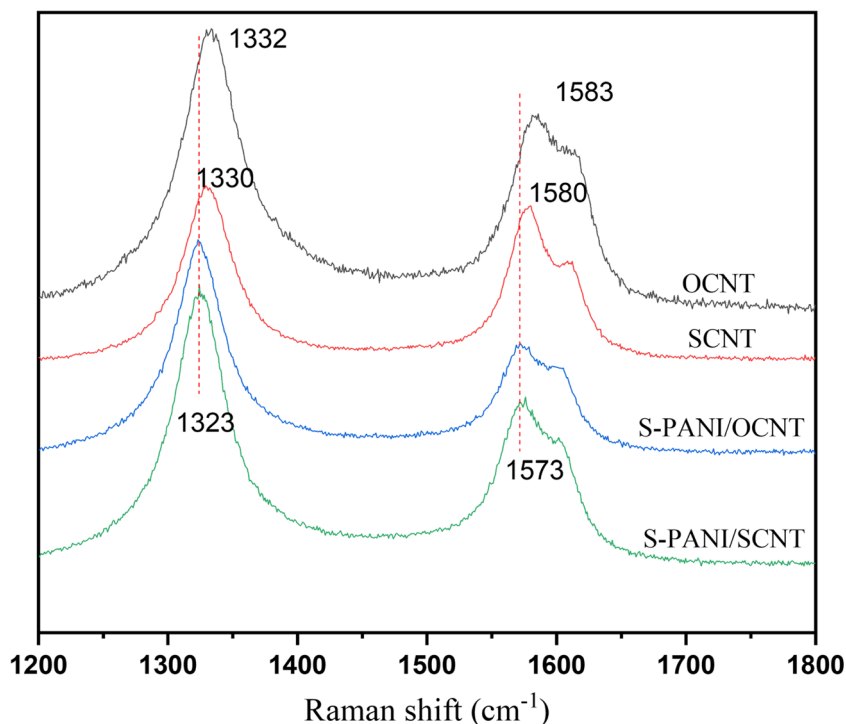


**Fig. 3** Raman spectra of OCNT, SCNT, S-PANI/OCNT, and S-PANI/SCNT



performance. The microscopic appearance is shown in Fig. 4a, b. It can be seen that S-PANI presents a two-phase structure as a whole, in which spherical NPES with a diameter of about 200 nm is dispersed in a uniform phase. PANI is a short rod-like morphology with a relatively regular structure, and the diameter of PANI nanorods is in the range of 60–100 nm. Figure 4c and d are SEM images of OCNT and S-PANI/OCNT, respectively. It can be observed from the figure that the diameter of OCNT is about 40–60 nm, and the whole presents a staggering disordered state with suitable porosity. This porous structure allows ions to be exchanged between the active material and the electrolyte more quickly. When OCNT and S-PANI were made into a composite, the tube diameter increased, due to S-PANI coating on the surface of OCNT. Besides, S-PANI coating can improve conductivity and associated transportation of charges, hence improving the electrochemical performance. Figure 4e and f are the microtopography of SCNT and S-PANI/SCNT, respectively, which are the same as OCNT and S-PANI/OCNT. S-PANI also formed a coating layer on the surface of SCNT, but the coating effect was relatively better. It is important to note that, the grafted polymer has not blocked the pores in the structure; hence the performance is not compromised. In contrast, the conventional mixing of the components results in the filling of polymer chains in the pores thus reduces the overall exposed area available for electrochemical reaction. The above phenomenon indicated that S-PANI was successfully polymerized on the surface of OCNT and SCNT, and CNT was coated and modified, and the corresponding nanocomposite material was successfully prepared.

Since MWCNTs adsorb ions in the electrolyte and form an electric double layer on the surface, we used the  $N_2$  isothermal adsorption and desorption method to test the pore structure and SSA of the composite materials. S-PANI/OCNT and S-PANI/SCNT in Fig. 5a shows the  $N_2$  adsorption/desorption isotherm and associated specific surface area is  $59.3 \text{ m}^2 \text{ g}^{-1}$  and  $63.6 \text{ m}^2 \text{ g}^{-1}$  for S-PANI/OCNT and S-PANI/SCNT, respectively. According to the international IUPAC standard, it can be judged that the  $N_2$  adsorption isotherm has type IV characteristics, indicating that the  $N_2$  molecules are adsorbed on the inner surface of the mesopores in the form of a single layer to multiple layers. Besides, it can be seen that the relative pressure  $P/P_0$  presented an obvious hysteresis in the range of 0.45–0.99, which is a typical characteristic of mesoporous materials, indicating that the sample has a mesoporous structure. Figure 5b shows the corresponding pore size distribution. The pore volumes of the samples S-PANI/OCNT and S-PANI/SCNT are  $0.39 \text{ cm}^3 \text{ g}^{-1}$  and  $0.31 \text{ cm}^3 \text{ g}^{-1}$ , respectively. By analyzing the pore size distribution map obtained from the desorption curve using BJH method, it can be seen that the pore size distribution of the two is in a wide range, i.e., 18–530 Å, as observed for mesoporous materials.

### Electrochemical performance analysis

The three-electrode system was used to test the electrochemical performance of composite materials. The S-PANI/OCNT and S-PANI/SCNT composite materials were used as working electrodes and 1 M,  $H_2SO_4$  as the electrolyte.

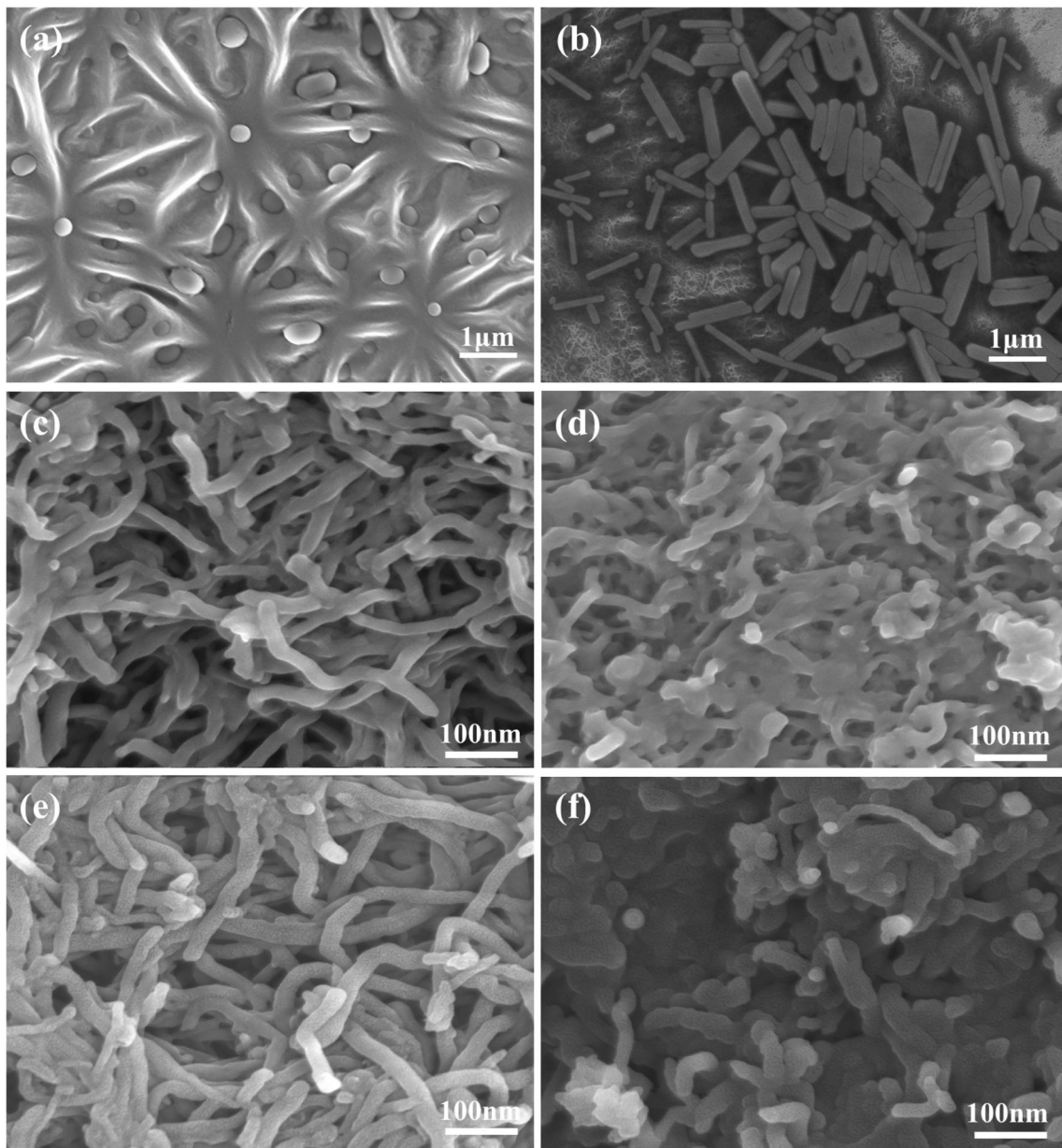
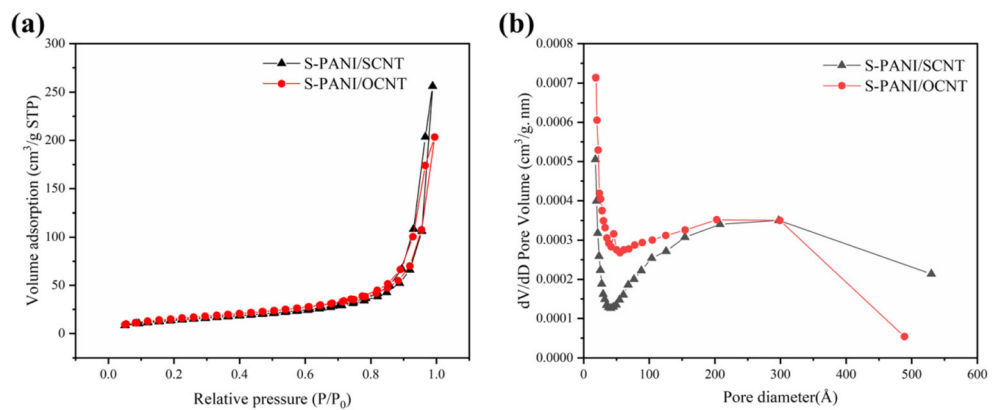


**Fig. 4** SEM images of **a**, **b** S-PANI, **c** OCNT, **d** S-PANI/OCNT, **e** SCNT, and **f** S-PANI/SCNT

**Fig. 5 a** Nitrogen adsorption/desorption isotherms and **b** Barrett-Joyner-Halenda (BJH) pore size distributions of the S-PANI/OCNT and S-PANI/SCNT composites



The cyclic voltammetry (CV) was performed to test the performance of S-PANI/OCNT and S-PANI/SCNT composite electrode as shown in Fig. 6a,b. From the corresponding CV curves, it can be observed that both curves have obvious redox peaks. This is because S-PANI in the composite material undergoes doping and reverse doping reactions during charge and discharge. As the scanning rate increases from 5 to 100  $\text{mV s}^{-1}$ , the corresponding current density was proportionally increased. The oxidation peaks of the two samples move towards the positive potential, and the reduction peaks move towards the negative potential. However, the shape of the CV plot remained unchanged, which indicates that our composite structure offers suitable porosity, hence performance was retained at high scan rates. Comparing the closed CV curve area of the two electrodes at the same scan rate, it can be seen that the CV curve area of S-PANI/SCNT is comparatively larger than S-PANI/OCNT. The higher integrated area of the Cv curve is related to the higher specific capacitance of S-PANI/SCNT. Comparatively better activity of S-PANI/SCNT can be due to higher defects imparted by the S-doped sites in CNT. Compared with oxygenated defects, the

sulfonated sites can cause higher lattice dislocations in the carbon skeleton due to their bigger size. Apart from the atomic size effect, the oxygen strongly withdraws the electron cloud from  $\text{sp}^2$ -hybridized skeleton of OCNTs, due to higher electronegativity. In contrast, the electronegativity difference between S and C is almost negligible; therefore, higher electron cloud density is expected in SCNT. Based on this assumption, we expect higher conductivity in SCNT. The S-doping is only contributing to the performance enhancement by changing the spin quantum number on the edge sites.

The normalized CV curves have been drawn which indicated pseudocapacitance and high rate performance of the S-PANI/SCNT electrode (Fig. 6c). At a low scan rate of 5  $\text{mV s}^{-1}$ , this electrode displayed a gravimetric capacitance of 310  $\text{F g}^{-1}$  and retained 81% of the initial capacitance at a scan rate of 100  $\text{mV s}^{-1}$  [47, 48].

The S-PANI/OCNT and S-PANI/SCNT electrodes were tested with electrochemical impedance spectroscopy (EIS) at a scanning frequency of 1–10,000 Hz (Fig. 6d). The real part and the imaginary part of the electrode impedance were estimated using the alternating current signal. The corresponding

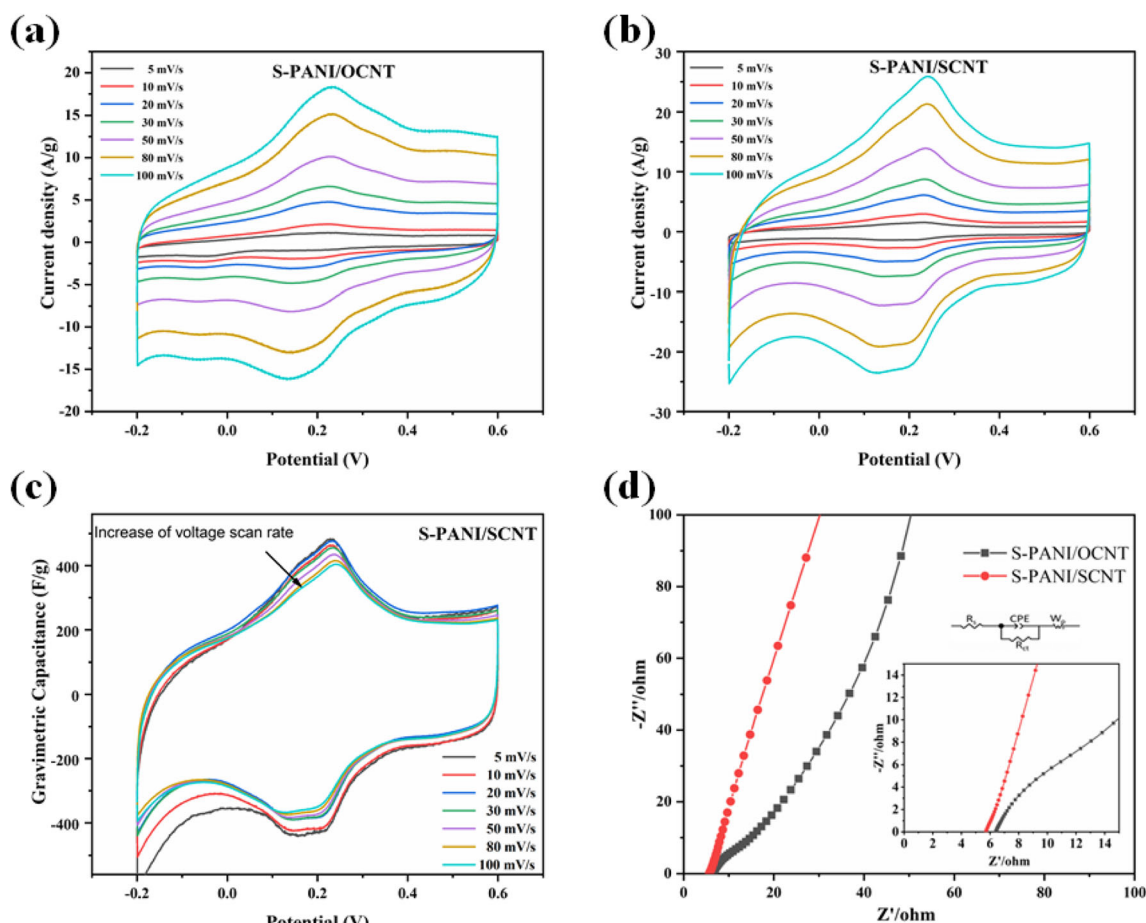


**Fig. 6** CV curves of **a** S-PANI/OCNT and **b** S-PANI/SCNT electrodes. **c** Gravimetric capacitance vs. potential curves at different scan rates. **d** EIS curves of S-PANI/SCNT and S-PANI/OCNT electrodes at the frequency

range of  $10^0$ – $10^5$  Hz. The inset shows the results at the high-frequency region and equivalent circuit



Nyquist AC impedance spectra were obtained by taking the real and imaginary impedance as the abscissa and ordinate, respectively. The equivalent series resistance of the working electrode is mainly composed of the contact resistance between the active material and the current collector, the electronic resistance, and the ionic resistance. The EIS of the S-PANI/OCNT and S-PANI/SCNT electrodes intersect the real axis at 6.3 Ω and 5.7 Ω in the high-frequency region (Fig. 6d), respectively. The equivalent series resistance of both electrodes was small, thus offering good conductivity. Besides, the projection length of the S-PANI/SCNT on the real axis is shorter than that of S-PANI/OCNT. Shorter projection length is due to impediments to the charge transfer and better reversible diffusion process. The linear part of the low-frequency region corresponds to the doping controlled by ion diffusion. The difference in EIS was consistent with the CV performance; hence it can be related to the conductivity difference of both S/O doping.

To better understand the enhanced electrochemical performances of the S-PANI/SCNT electrode, the resistance, and charge transfer mechanism at the electrode-electrolyte interface of S-PANI/SCNT and S-PANI/OCNT electrodes, EIS test is conducted at the open-circuit potential within the

frequency range of 10<sup>0</sup>–10<sup>5</sup> Hz. Figure 6d demonstrates the Nyquist plots of S-PANI/SCNT and S-PANI/OCNT electrodes. Both the plots comprise of two portions, semicircles in the high-frequency region and slope along vertical Y-axis, respectively. The inherent material resistance, electrolyte ionic resistance, and electrode-electrolyte contact resistance (*R<sub>s</sub>*) are obtained from the intercept of real values (*Z'*) at the high-frequency regions [49]. The charge transfer resistance (*R<sub>ct</sub>*) is obtained from the semicircle at the high-frequency region, which corresponds to the resistance during electron transfer at the electrode-electrolyte interface. An analysis of the Nyquist plots using corresponding circuits shows that the SPANI-SCNT offers low *R<sub>s</sub>* (5.6 Ω) and *R<sub>ct</sub>* (0.8 Ω) compared with large values of *R<sub>s</sub>* (6.5 Ω) and *R<sub>ct</sub>* (14.5 Ω) for SPANI-OCNT electrode. The low *R<sub>s</sub>* and *R<sub>ct</sub>* values of the S-PANI/SCNT electrode suggest that the composite material facilitates fast diffusion of electrolyte ions and advantageous to the long-term stability of the electrode.

The S-PANI/OCNT and S-PANI/SCNT working electrodes were subjected to constant current charge and discharge tests, with −0.2–0.6 V as the potential window, at a current density of 1–10 A g<sup>−1</sup> (Fig. 7). By measuring the relationship between electrode potential and charge and discharge time, it

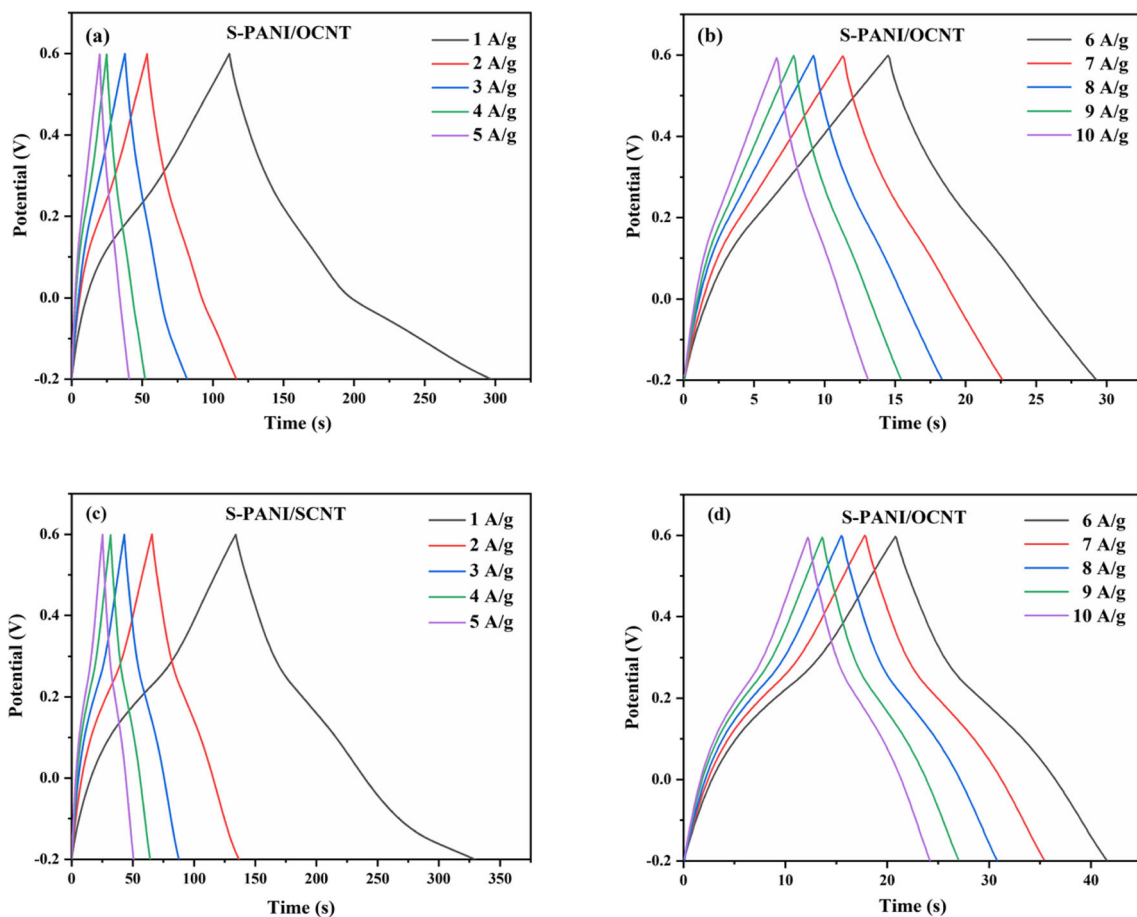
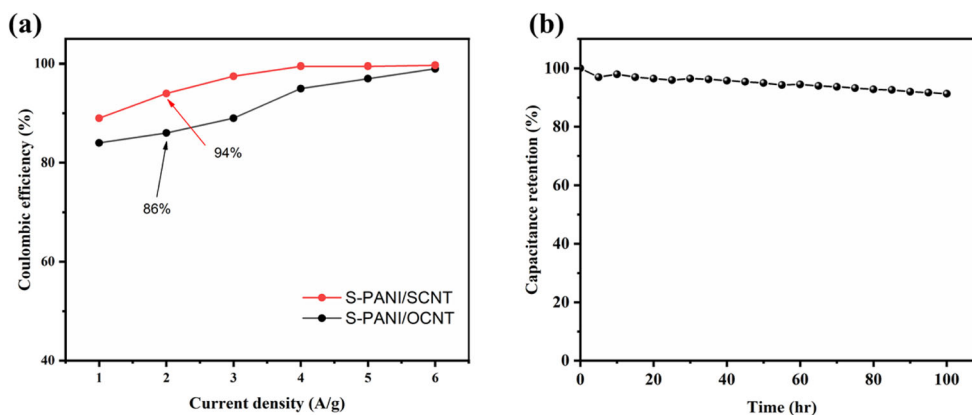


Fig. 7 Galvanostatic charge-discharge curves of a, b S-PANI/OCNT and c, d S-PANI/SCNT electrode at different current densities

**Fig. 8** **a** Coulombic efficiency versus current density of S-PANI/SCNT and S-PANI/OCNT electrodes. **b** Float voltage stability test of the S-PANI/CNT electrode for 100 h



can be seen that the constant current charge and discharge curves of the two electrode materials at different current densities all present a relatively symmetrical inverted triangle shape, showing significant electric double-layer capacitor characteristics. The specific capacitance of the working electrode can be calculated according to the charge-discharge curve of constant current by using Equation 1.

$$C = I\Delta t/m\Delta V \quad (1)$$

where  $I$  is the electrode current,  $\Delta t$  is the discharge time,  $m$  is the mass of the active material, and  $\Delta V$  is the potential difference that excludes the voltage drop during the discharge. Comparing the constant current charge-discharge curves of the two samples at a current density of  $1 \text{ A g}^{-1}$ , the calculation using the above equation shows that the S-PANI/SCNT electrode has a longer charge-discharge time, with a specific capacitance of  $345.4 \text{ F g}^{-1}$ . It is higher than the specific capacitance of the S-PANI/OCNT electrode ( $316.8 \text{ F g}^{-1}$ ), which is consistent with the analysis result of the CV curve. Based on the above analysis, we could contemplate that different ways of functionalizing CNT had a certain degree of influence on the electrochemical performance of composite electrodes. Also, density of O/S doping affects the active groups available for crosslinking of carbon nanotubes and S-PANI.

**Fig. 9** **a** Specific capacitance of S-PANI/OCNT and S-PANI/SCNT electrodes with current density ranging from 1 to  $10 \text{ A g}^{-1}$ . **b** Electrochemical stability at a current density of  $5 \text{ A g}^{-1}$  over 5000 cycles

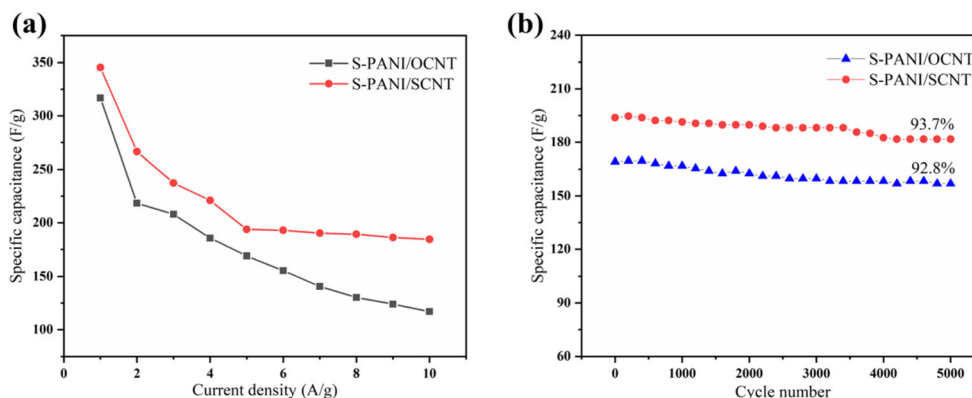


Figure 8a shows that the Coulombic efficiencies of S-PANI/SCNT and S-PANI/OCNT electrodes. As the current density increases from  $1$  to  $6 \text{ A g}^{-1}$  the Coulombic efficiency of the S-PANI/SCNT electrode increases from 89 to 99.7% with a negligible IR drop, whereas the CE of S-PANI/OCNT is 84 and 99% at current densities of  $1$  and  $6 \text{ A g}^{-1}$ , respectively. The high Coulombic efficiency confirms the excellent charge/discharge reversibility of the SPANI-SCNT electrode due to high conductivity and high ion diffusion pathways of the fibrillar network, even with a high gravimetric capacitance of  $345.4 \text{ F g}^{-1}$  [50, 51].

A voltage holding stability test was performed at a constant voltage of  $0.6 \text{ V}$  that was applied to an assembled supercapacitor electrode (S-PANI/SCNT) in  $1 \text{ M H}_2\text{SO}_4$  electrolyte for 100 h. Two charges/discharge cycles from  $-0.2$  to  $0.6 \text{ V}$  were performed at a constant current density of  $2.5 \text{ A g}^{-1}$  every 5 h to enumerate the corresponding retaining specific capacitance. S-PANI/CNT electrode displays exceptional stability with only a 10% loss of capacitance. The graph between the time and capacitance retention is shown in Fig. 8b [52].

According to the constant current charge and discharge curves of S-PANI/OCNT and S-PANI/SCNT electrodes, the capacitance values at the current density of  $1$ – $10 \text{ A g}^{-1}$  were calculated. The associated curve of rate performance is given in Fig. 9a. The increase in current density causes a decrease in

the capacitance of both electrodes. When the current density increased to  $10 \text{ A g}^{-1}$ , the specific capacitance of the S-PANI/OCNT electrode dropped to  $117 \text{ F g}^{-1}$  from  $316.8 \text{ F g}^{-1}$  which was obtained at a current density of  $1 \text{ A g}^{-1}$ . Besides, the capacitance of the S-PANI/SCNT electrode was higher than S-PANI/OCNT electrode under different current densities. The calculated capacitance is  $345.4 \text{ F g}^{-1}$  at current densities of  $1 \text{ A g}^{-1}$ , and  $184.5 \text{ F g}^{-1}$  at  $10 \text{ A g}^{-1}$ . It can be seen that the rate performance of the S-PANI/SCNT electrode is better, which is related to the structural regularity of the electrode. Both samples were subjected to 5000 cycles of constant current charge and discharge tests at a current density of  $5 \text{ A g}^{-1}$ , and the corresponding cycle stability diagrams are shown in Fig. 9b. Generally, PANI undergoes redox reactions during repeated charging and discharging, which leads to the destruction of its molecular chain structure. However, the S-PANI made by NPES grafting has excellent conductivity and ionic affinity, so it endows the composite electrode material with comparatively better cycle stability. Both S-PANI/OCNT and S-PANI/SCNT have excellent cycle stability and retained more 90% of initial performance after 5000 cycles. Besides, it can be seen that the specific capacitance of the S-PANI/SCNT working electrode is always higher than that of the S-PANI/OCNT during the cycle. Better performance results from higher regularity of the S-PANI/SCNT microstructure, which is also responsible for superior electrochemical performance.

## Conclusion

In this study, a unique S-PANI was prepared by doping long-chain protonic acid during in situ polymerization. Oxidation and sulfonation of MWCNTs were carried out to generate active groups for in situ grafting of S-PANI on the surface. The S-PANI/OCNT and S-PANI/SCNT composites were used as working electrodes, and detailed structural and electrochemical characterization was performed. The FTIR and XRD tests show that the functional treatment of the CNT surface has successfully grafted the corresponding functional groups, and S-PANI was successfully grafted on the surface of OCNT and SCNT. The S-PANI resulted in uniform dispersion and enhanced pseudopotentiability. The CV curves of both electrodes have good reversible charge-discharge properties, and both exhibit pseudocapacitance, essentially provided by the conductive polymer in the composite material. The S-PANI/OCNT and S-PANI/SCNT electrodes were subjected to constant current charge and discharge tests at a current density of  $1 \text{ A g}^{-1}$ , and the specific capacities obtained were  $316.8 \text{ F g}^{-1}$  and  $345.4 \text{ F g}^{-1}$ , respectively. After 5000 consecutive charge-discharge cycles at a current density of  $5 \text{ A g}^{-1}$ , the capacitance retention rates were all above 92%. S-PANI composited functionalized MWCNTs showed decent specific

capacities and cyclic stability. The performance of S-PANI/SCNT was better than S-PANI/OCNT, which is evident that a suitable dopant for MWCNTs' activation is important to achieve higher performance. We believe that our proposed system is suitable for other electrochemical energy harvesting (solar cells) and energy storage (secondary battery) devices.

**Funding** The study was supported by the National Natural Science Foundation of China (No. 51673154, 51703177).

## Declarations

**Conflict of interest** The authors declare that they have no conflict to declare.

## References

- Zhu J, Huang B, Zhao C, Xu H, Wang S, Chen Y, Xie L, Chen L (2019) Benzoic acid-assisted substrate-free synthesis of ultrathin nanosheets assembled two-dimensional porous  $\text{Co}_3\text{O}_4$  thin sheets with 3D hierarchical micro-/nano-structures and enhanced performance as battery-type materials for supercapacitors. *Electrochim Acta* 313:194–204. <https://doi.org/10.1016/j.electacta.2019.05.019>
- Swaminathan A, Ravi R, Sasikumar M, Dasaiah M, Hirankumar G, Ayyasamy S (2020) Preparation and characterization of PVA/PAM/ $\text{NH}_4\text{SCN}$  polymer film by ultrasound-assisted solution casting method for application in electric double layer capacitor. *Ionics* 26(8):4113–4128. <https://doi.org/10.1007/s11581-020-03542-4>
- Rashti A, Wang B, Hassani E, Feyzbar-Khalkhali-Nejad F, Zhang X, Oh T-S (2020) Electrophoretic deposition of nickel cobaltite/polyaniline/rGO composite electrode for high-performance all-solid-state asymmetric supercapacitors. *Energy Fuel* 34(5):6448–6461. <https://doi.org/10.1021/acs.energyfuels.0c00408>
- Iqbal J, Numan A, Ansari MO, Jagadish PR, Jafer R, Bashir S, Mohamad S, Ramesh K, Ramesh S (2020) Facile synthesis of ternary nanocomposite of polypyrrole incorporated with cobalt oxide and silver nanoparticles for high performance supercapattery. *Electrochim Acta* 348:136313. <https://doi.org/10.1016/j.electacta.2020.136313>
- Jiang X, Shi G, Wang G, Mishra P, Du J, Zhang Y (2020)  $\text{Fe}_2\text{O}_3$ /hemp straw-based porous carbon composite for supercapacitor electrode materials. *Ionics* 26(8):4039–4051. <https://doi.org/10.1007/s11581-020-03547-z>
- Wei L, Wu M, Yan M, Liu S, Cao Q, Wang H (2019) A review on electrothermal modeling of supercapacitors for energy storage applications. *IEEE J Emerg Sel Top Power Electron* 7(3):1677–1690. <https://doi.org/10.1109/jestpe.2019.2925336>
- Zhou S, Liu Y, Yan M, Sun L, Luo B, Yang Q, Shi W (2020) Design of  $\text{FeCo}_2\text{S}_4$ @ $\text{Ni}(\text{OH})_2$  core-shell hollow nanotube arrays on carbon paper for ultra-high capacitance in supercapacitors. *Electrochim Acta* 349:136337. <https://doi.org/10.1016/j.electacta.2020.136337>
- Yue X-M, Liu Z-J, Xiao C-C, Ye M, Ge Z-P, Peng C, Gu Z-Y, Zhu J-S, Zhang S-Q (2020) Synthesis of  $\text{Co}_3\text{O}_4$ /reduced graphene oxide by one step-hydrothermal and calcination method for high-performance supercapacitors. *Ionics*. 27:339–349. <https://doi.org/10.1007/s11581-020-03797-x>
- Zhou S, Ye Z, Hu S, Hao C, Wang X, Huang C, Wu F (2018) Designed formation of  $\text{Co}_3\text{O}_4$ / $\text{ZnCo}_2\text{O}_4$ / $\text{CuO}$  hollow polyhedral nanocages derived from zeolitic imidazolate framework-67 for

- high-performance supercapacitors. *Nanoscale* 10(33):15771–15781. <https://doi.org/10.1039/c8nr05138k>
10. Wang X, Chen L, Zhang S, Chen X, Li Y, Liu J, Lu F, Tang Y (2019) Compounding  $\delta$ -MnO<sub>2</sub> with modified graphene nanosheets for highly stable asymmetric supercapacitors. *Colloids Surf A Physicochem Eng Asp* 573:57–66. <https://doi.org/10.1016/j.colsurfa.2019.04.040>
  11. Gong Y, Li D, Fu Q, Zhang Y, Pan C (2020) Nitrogen self-doped porous carbon for high-performance supercapacitors. *ACS Appl Energy Mater* 3(2):1585–1592. <https://doi.org/10.1021/acsaem.9b02077>
  12. Hui X, Qian L, Harris G, Wang T, Che J (2016) Fast fabrication of NiO@graphene composites for supercapacitor electrodes: combination of reduction and deposition. *Mater Des* 109:242–250. <https://doi.org/10.1016/j.matdes.2016.07.072>
  13. Yadong TH, Yahui W, Chen L, Xiaoliang W (2019) Fe<sub>2</sub>O<sub>3</sub> nanoparticles decorated on graphene-carbon nanotubes conductive networks for boosting the energy density of all-solid-state asymmetric supercapacitor. *ACS Sustainable Chem Eng* April 28, 2019. <https://doi.org/10.1021/acssuschemeng.8b06857>
  14. Eskusson PR, Nerut J, and J'anes A (2016) A hybrid capacitor based on Fe<sub>3</sub>O<sub>4</sub>-graphene nanocomposite/few-layer graphene in different aqueous electrolytes. *J Electrochem Soc* 163 (13) A2768-A2775. doi:<https://doi.org/10.1149/2.1161613jes>
  15. Poonam SK, Arora A, Tripathi SK (2019) Review of supercapacitors: materials and devices. *J Energy Stor* 21:801–825. <https://doi.org/10.1016/j.est.2019.01.010>
  16. Liu H, Liu X, Wang S, Liu H-K, Li L (2020) Transition metal based battery-type electrodes in hybrid supercapacitors: a review. *Energy Stor Mater* 28:122–145. <https://doi.org/10.1016/j.ensm.2020.03.003>
  17. Guo D, Song X, Li F, Tan L, Ma H, Zhang L, Zhao Y (2018) Oriented synthesis of Co<sub>3</sub>O<sub>4</sub> core-shell microspheres for high-performance asymmetric supercapacitor. *Colloids Surf A Physicochem Eng Asp* 546:1–8. <https://doi.org/10.1016/j.colsurfa.2018.02.072>
  18. Ates M, Mizrak I, Kuzgun O, Aktas S (2020) Synthesis, characterization, and supercapacitor performances of activated and inactivated rGO/MnO<sub>2</sub> and rGO/MnO<sub>2</sub>/PPy nanocomposites. *Ionics* 26(9):4723–4735. <https://doi.org/10.1007/s11581-020-03605-6>
  19. Kong S, Cheng K, Ouyang T, Gao Y, Ye K, Wang G, Cao D (2017) Facile dip coating processed 3D MnO<sub>2</sub>-graphene nanosheets/MWNT-Ni foam composites for electrochemical supercapacitors. *Electrochim Acta* 226:29–39. <https://doi.org/10.1016/j.electacta.2016.12.158>
  20. Keawpoy N, Venkatkarthick R, Wangyao P, Zhang X, Liu R, Qin J (2020) Eco-friendly conductive cotton-based textile electrodes using silver- and carbon-coated fabrics for advanced flexible supercapacitors. *Energy Fuel* 34(7):8977–8986. <https://doi.org/10.1021/acsc.energyfuels.0c01419>
  21. Yadav HM, Ramesh S, Kumar KA, Shinde S, Sandhu S, Sivasamy A, Shrestha NK, Kim HS, Kim H-S, Bathula C (2020) Impact of polypyrrole incorporation on nickel oxide@multi walled carbon nanotube composite for application in supercapacitors. *Polym Test* 89:106727. <https://doi.org/10.1016/j.polymertesting.2020.106727>
  22. Liang X, Cheng Q (2018) Synergistic reinforcing effect from graphene and carbon nanotubes. *Compos Commun* 10:122–128. <https://doi.org/10.1016/j.coco.2018.09.002>
  23. Yang Z, Xiang M, Wu Z, Hui J, Huang Q, Zhang J, Qin H (2020) A three-dimensional carbon electrode derived from bean sprout for supercapacitors. *Ionics* 26(11):5705–5714. <https://doi.org/10.1007/s11581-020-03682-7>
  24. Tian F, Zhong S, Nie W, Zeng M, Chen B, Liu X (2020) Multi-walled carbon nanotubes prepared with low-cost Fe-Al bimetallic catalysts for high-rate rechargeable Li-ion batteries. *J Solid State Electrochem* 24(3):667–674. <https://doi.org/10.1007/s10008-020-04502-8>
  25. Karade SS, Raut SS, Gajare HB, Nikam PR, Sharma R, Sankapal BR (2020) Widening potential window of flexible solid-state supercapacitor through asymmetric configured iron oxide and poly(3,4-ethylenedioxythiophene) polystyrene sulfonate coated multi-walled carbon nanotubes assembly. *J Energy Stor* 31: 101622. <https://doi.org/10.1016/j.est.2020.101622>
  26. Liu X, Xue L, Lu Y, Xia Y, Li Q (2020) Fabrication of polypyrrole/multi-walled carbon nanotubes composites as high performance electrodes for supercapacitors. *J Electroanal Chem* 862:114006. <https://doi.org/10.1016/j.jelechem.2020.114006>
  27. Yang L, Yang Y, Wang S, Guan X, Guan X, Wang G (2020) Multi-heteroatom-doped carbon materials for solid-state hybrid supercapacitors with a superhigh cycling performance. *Energy Fuel* 34(4):5032–5043. <https://doi.org/10.1021/acs.energyfuels.9b04505>
  28. Lu Z, Raad R, Safaei F, Xi J, Liu Z, Foroughi J (2019) Carbon nanotube based fiber supercapacitor as wearable energy storage. *Front Mater* 6. doi:<https://doi.org/10.3389/fmats.2019.00138>
  29. Wang H, Liang L, Duan L, Sun S, Cheng X (2019) Fabrication of MWNT@CMPs and carbonized MWNT@CMPs for supercapacitors. *Mater Chem Phys* 226:309–317. <https://doi.org/10.1016/j.matchemphys.2019.01.036>
  30. Wang Z, Liu C, Shi G, Wang G, Zhang Q, Zhang H, Su Y, Yu J, Li X, Luo F, Hu Y, Yi K (2020) Electrospinning CoS<sub>2</sub>/carbon nanofibers with enhanced stability as electrode materials for supercapacitors. *Ionics* 26(11):5737–5746. <https://doi.org/10.1007/s11581-020-03725-z>
  31. Shang Y, Ma S, Wei Y, Yang H, Xu Z (2020) Flower-like ternary metal of Ni-Co-Mn hydroxide combined with carbon nanotube for supercapacitor. *Ionics* 26(7):3609–3619. <https://doi.org/10.1007/s11581-020-03496-7>
  32. Qian Y (2016) Facile PVP-assisted synthesis of MnO<sub>2</sub>@MWNT composites and their application in supercapacitors. *International Journal of Electrochemical Science*:7453-7460. doi:<https://doi.org/10.1007/10.20964/2016.09.45>
  33. Ayman I, Rasheed A, Ajmal S, Rehman A, Ali A, Shakir I, Warsi MF (2020) CoFe<sub>2</sub>O<sub>4</sub> nanoparticle-decorated 2D MXene: a novel hybrid material for supercapacitor applications. *Energy Fuel* 34(6): 7622–7630. <https://doi.org/10.1021/acs.energyfuels.0c00959>
  34. Sahebani S, Zebarjad SM, Vahdati Khaki J, Lazzeri A (2016) The decoration of multi-walled carbon nanotubes with nickel oxide nanoparticles using chemical method. *Int Nano Lett* 6(3):183–190. <https://doi.org/10.1007/s40089-016-0185-8>
  35. Lee KS, Shin MJ, Park CW, Kim J-D (2018) Simple and direct synthesis of ZnO decorated multi-walled carbon nanotube for supercapacitor electrodes. *Colloids Surf A Physicochem Eng Asp* 538:23–27. <https://doi.org/10.1016/j.colsurfa.2017.10.075>
  36. Lee KS, Park M, Ko JM, Kim J-D (2016) Electrochemical properties of multi-walled carbon nanotubes treated with nitric acid for a supercapacitor electrode. *Colloids Surf A Physicochem Eng Asp* 506:664–669. <https://doi.org/10.1016/j.colsurfa.2016.07.044>
  37. Yan P, Yan L, Gao J, Zhang Z, Gong G, Hou M (2020) Nitrogen and fluorine co-doped graphene hydrogel for high-performance supercapacitors. *Ionics* 26(9):4705–4712. <https://doi.org/10.1007/s11581-020-03593-7>
  38. Ho K-C, Lin L-Y (2019) A review of electrode materials based on core-shell nanostructures for electrochemical supercapacitors. *J Mater Chem A* 7(8):3516–3530. <https://doi.org/10.1039/c8ta11599k>
  39. Gao B, He D, Yan B, Suo H, Zhao C (2015) Flexible carbon cloth based polypyrrole for an electrochemical supercapacitor. *J Mater Sci Mater Electron* 26(9):6373–6379. <https://doi.org/10.1007/s10854-015-3225-7>

40. He X, Chen H, Xu C, Fan J, Xu W, Li Y, Deng H, Shen J (2020) Ratiometric and colorimetric fluorescent probe for hypochlorite monitor and application for bioimaging in living cells, bacteria and zebrafish. *J Hazard Mater* 388:122029. <https://doi.org/10.1016/j.jhazmat.2020.122029>
41. Tahir M, He L, Yang W, Hong X, Haider WA, Tang H, Zhu Z, Owusu KA, Mai L (2020) Boosting the electrochemical performance and reliability of conducting polymer microelectrode via intermediate graphene for on-chip asymmetric micro-supercapacitor. *J Energy Chem* 49:224–232. <https://doi.org/10.1016/j.jechem.2020.02.036>
42. Akbar AR, Tian W, Qadir MB, Khaliq Z, Liu Z, Tahir M, Hu Y, Xiong C, Yang Q (2020) A novel ternary composite aerogel for high-performance supercapacitor. *Colloids and Surfaces A: Physicochemical and Engineering Aspects*:125644. doi:<https://doi.org/10.1016/j.colsurfa.2020.125644>
43. Jin L, Jiang Y, Zhang M, Li H, Xiao L, Li M, Ao Y (2018) Oriented polyaniline nanowire arrays grown on dendrimer (PAMAM) functionalized multiwalled carbon nanotubes as supercapacitor electrode materials. *Sci Rep* 8(1):6268. <https://doi.org/10.1038/s41598-018-24265-7>
44. Ibrahim A, Abdel-Aziz MH, Zoromba MS, Al-Hossainy AF (2018) Structural, optical, and electrical properties of multi-walled carbon nanotubes/polyaniline/Fe<sub>3</sub>O<sub>4</sub> ternary nanocomposites thin film. *Synth Met* 238:1–13. <https://doi.org/10.1016/j.synthmet.2018.02.006>
45. Dawouda HD, Altahtamounia TM, Zaghoa MM, Bensalahb N (2017) A brief overview of flexible CNT/PANI super capacitors. *Materials Science and Nanotechnology* 01 (02). doi:10.35841/nanotechnology.1.2.23-36
46. Huang J, Li Q, Wang Y, Wang Y, Dong L, Xie H, Xiong C (2011) Self-suspended polyaniline doped with a protonic acid containing a polyethylene glycol segment. *Chem Asian J* 6(11):2920–2924. <https://doi.org/10.1002/asia.201100437>
47. Thierry Brousse DBE, Jeffrey WL (2015) To be or not to be pseudocapacitive? *J Electrochem Soc* 162(5). <https://doi.org/10.1149/2.0201505jes>
48. Tee ITE, Thomberg T, Jänes A, Lust E (2016) Supercapacitors based on activated silicon carbide-derived carbon materials and ionic liquid. *J Electrochem Soc* 163(7). <https://doi.org/10.1149/2.0931607jes>
49. Hallik A, Alumaa A, Tamm J, Sammelselg V, Väärtnõu M, Jänes A, Lust E (2006) Analysis of electrochemical impedance of polypyrrole/sulfate and polypyrrole/perchlorate films. *Synth Met* 156(5-6):488–494. <https://doi.org/10.1016/j.synthmet.2006.02.004>
50. Laheäär A, Przygocki P, Abbas Q, Béguin F (2015) Appropriate methods for evaluating the efficiency and capacitive behavior of different types of supercapacitors. *Electrochem Commun* 60:21–25. <https://doi.org/10.1016/j.elecom.2015.07.022>
51. Thomberg T, Lust E, Jänes A (2020) Iodide ion containing ionic liquid mixture based asymmetrical capacitor performance. *J Energy Stor* 32:101845. <https://doi.org/10.1016/j.est.2020.101845>
52. Weingarth D, Foelske-Schmitz A, Kötz R (2013) Cycle versus voltage hold—which is the better stability test for electrochemical double layer capacitors? *J Power Sources* 225:84–88. <https://doi.org/10.1016/j.jpowsour.2012.10.019>

**Publisher's note** Springer Nature remains neutral with regard to jurisdictional claims in published maps and institutional affiliations.